Physical Chemistry: An Indian Journal

Research | Special issue

Significant CO_2 Adsorption Ability of Nanoscale $BaTiO_3$ Ceramics Fabricated by Carbon-Template-Solvothermal Reactions

Takumi Watanabe, Sharif Md Khan, Hirofumi Kanoh, and Tomonori Ohba*

Graduate School of Science, Chiba University, 1-33 Yayoi, Inage, Chiba 2638522, Japan

***Corresponding author:** Ohba T, Graduate School of Science, Chiba University, 1-33 Yayoi, Inage, Chiba 2638522, Japan, E-mail: ohba@chiba-u.jp

Received: March 29, 2017; **Accepted:** April 21, 2017; **Published:** April 28, 2017

©Abstract

Separation of CO_2 using adsorption and membrane separations can be performed under moderate conditions for carbon capture and release processes. Although porous media work well for this purpose, these novel materials must be fabricated with high CO_2 separation ability. We propose the use of nanoscale $BaTiO_3$ crystals as separators for CO_2 adsorption. Although $BaTiO_3$ is a conventional ceramic, it exhibits high dielectric properties and shows potential for a strong interaction with the quadrupole moment of CO_2. However, this high adsorption potential is reduced by the extremely small surface area of $BaTiO_3$. Here, we fabricated nanoscale $BaTiO_3$ crystals with high surface area and nanopores, and demonstrated their excellent CO_2 adsorption performance with large adsorption hysteresis. The CO_2 adsorbed in the nanoscale $BaTiO_3$ crystals could be perfectly released under vacuum conditions. The structure of adsorbed CO_2 was similar to CO_2 solid at 1 GPa. The unique adsorption properties of CO_2 in these nanoscale $BaTiO_3$ crystals are of interest for the development of materials with high CO_2 adsorption ability.

Keywords: ***CO_2 adsorption; Adsorption hysteresis; Barium titanate; Carbon storage; Nanoceramics; Chemisorption***

Introduction

The effects of global warming and climate change are receiving increasing attention [1,2]. In particular, emphasis has been placed on the control of CO_2 emissions, the main source of which is generally fossil fuel combustion [3,4]. The selection of an appropriate technology for CO_2 capture depends on many factors such as the partial pressure of CO_2 in the gas stream, recyclability, sensitivity to impurities, capital and operating costs, and environmental impact [2]. Based on the methods used for the separation of the components of a gas stream, absorption, adsorption, cryogenic distillation, or membrane purification can be applied for CO_2 capture [5]. Liquid absorbents need to be changed and may be corrosive and toxic, cryogenic distillation is a costly process, and membranes are efficient for the separation of relatively high concentrations of adsorbate. Therefore, of these four technologies, we focused on adsorption, which is desirable because of the easy recovery of the adsorbent using temperature or pressure fluctuations, thereby reducing the cost and energy consumption [5-8]. Suitable

Citation: Watanabe T, Md Khan S, Kanoh H, et al. Significant CO_2 Adsorption Ability of Nanoscale $BaTiO_3$ Ceramics Fabricated by Carbon-Template-Solvothermal Reactions. Phys Chem Ind J. 2017;S1:101.

adsorbents should exhibit high adsorption capacity, fast adsorption and desorption kinetics, recovery capabilities, and stability under various operating conditions [6,8,9]. In recent decades, adsorption using porous materials has been investigated. Porous materials are generally used for CO_2 capture because of their large surface area, and these materials are sometimes modified using functional groups, such as zeolites [10], activated carbon [11,12], and metal–organic frameworks [13], to increase the CO_2 adsorption capacity. Amine-modified silica is also used as an adsorbent that functions based on chemical interaction such as chemisorption [14].

Barium titanate ($BaTiO_3$) is a representative advanced ceramic and exhibits electronic properties that are useful for capacitors and sensors. $BaTiO_3$ is also a ferroelectric and thus exhibits spontaneous polarization; in addition, its surface has strong electrostatic interaction with several types of adsorbates, described by Coulomb's law for partial charges. Zhao et al. investigated the effect of ferroelectric polarization on the adsorption of 2-fluoroethanol and ethanol on $BaTiO_3$, suggesting reaction sites on polarized surfaces of $BaTiO_3$ [15,16]. Higai proposed dissociative adsorption of H_2O, and both H_2O and CO_2 were greatly stabilized on nanoscale $BaTiO_3$ according to first-principles calculations [17-19]. Baniecki et al. experimentally evaluated the CO_2 adsorption observed in defective surfaces of $BaTiO_3$.defective surfaces, they have received considerable attention not only for their use in electronic devices but also as adsorbents. Many researchers have investigated methods to reduce the size of $BaTiO_3$ using hydrothermal methods [20-22], sol-gel solvothermal methods [23,24], and template synthesis [24,25]. We previously fabricated nanoscale BaTiO3 crystals using carbon template-solvothermal reactions [26].

In this study, we adopted nanoscale $BaTiO_3$ crystals as CO_2 adsorbents and evaluated the performance of CO_2 adsorption on various sized $BaTiO_3$ crystals. In addition, the CO_2 adsorption mechanism and structures were investigated using adsorption isotherms at 273 K to 363 K and X-ray diffraction (XRD).

Materials and Methods

$BaTiO_3$ crystals of three different scales were prepared using solid-state, solvothermal, and carbon template-solvothermal reactions, and the resulting crystals were labeled macro-, meso-, and nano-$BaTiO_3$ crystals, respectively. The reagents used for the solid-state reaction were barium carbonate (>98%, Wako Pure Chemical Industries, Co. Ltd., Osaka, Japan) and rutile-type titanium dioxide (>99%, Wako Pure Chemical Industries, Co. Ltd.) A stoichiometric mixture of barium carbonate and titanium dioxide was pelletized under more than 60 MPa for 1 h, and the pellet obtained was heated at 1073 K for 24 h and subsequently heated at 1473 K for 48 h after grinding and pelletizing. In the solvothermal and carbon-template solvothermal reactions, barium ethoxide (>99%, Kojundo Chemical Laboratory Co. Ltd., Saitama, Japan) and titanium tetraisopropoxide (>99%, Kojundo Chemical Laboratory Co. Ltd.) were mixed with methanol (>99%, Wako Pure Chemical Industries, Co. Ltd.) and methoxyethanol (>99%, Wako Pure Chemical Industries, Ltd.). The volume ratio of methanol and methoxyethanol was 3:2. This solution was stirred vigorously for 3 h. After stirring, water or activated carbon fiber (W15, Ad'all Co. Ltd., Kyoto, Japan) adsorbed water was added into the precursor and heated at 400 K for 24 h for the solvothermal or carbon-template solvothermal reaction, respectively. Here, water-adsorbed activated carbon fibers were prepared by exposure to water vapor at 85–89% humidity. The meso-$BaTiO_3$ crystal after the solvothermal reaction was collected by centrifugation at 10000 rpm for 20 min. Nano-$BaTiO_3$ crystal was obtained by heat removal of the activated carbon fibers in an O_2 atmosphere at 673 K for 48 h. The products were purified by filtration using hot water to remove the precursors and

impurities. Two concentrations of Ba and Ti ions, 0.2 and 0.4 mol L^{-1}, were selected for both the solvothermal and carbon-template solvothermal reactions.

The structures of the $BaTiO_3$ crystals were evaluated using XRD (UltimaIV, Rigaku Co., Tokyo, Japan) with Cu Kα radiation (λ=0.1541 nm) at 40 kV and 40 mA and N_2 adsorption measurements at 77 K (Autosorb-1, Quantachrome Co., Florida, USA). The crystallite sizes of the $BaTiO_3$ crystals were determined using the Scherrer equation based on the XRD results [27]. The specific surface areas and micropore volumes were analyzed using the Brunauer-Emmett-Teller and Dubinin-Radushkevich equations, respectively [28,29]. The pore size distributions of the $BaTiO_3$ crystals were evaluated using non-local density functional theory calculations using the software package (Autosorb-1) [30,31]. The particle size was evaluated based on the spherical assumption. Particle structures were evaluated using transmission electron microscopy (TEM; JEM-2100F, JEOL Co., Tokyo, Japan) at 200 kV. Finally, the CO_2 sorption performances at 273, 303, 333, and 363 K were evaluated using adsorption measurements.

Results and Discussion

The crystal structure of the macro-$BaTiO_3$ crystal shown in FIG. 1a, matched well with that previously reported for $BaTiO_3$ (JCPDS Card #50626). The XRD patterns for the meso-$BaTiO_3$ crystal in FIG. 1a, perfectly correspond with those of the macro-$BaTiO_3$ crystal but were broadened because of the reduced crystallite size. Further broadening was observed for the nano-$BaTiO_3$ crystal, indicating nano-crystallization. The crystallite sizes of the macro-, meso-, and nano-$BaTiO_3$ crystals were calculated to be 370 nm, 13 nm ± 1 nm, and 6.4 nm ± 0.2 nm, respectively, using the Scherrer equation. Crystallite size evaluation using the Scherrer equation is known to be erroneous for crystals larger than 100 nm; the crystal size of the macro-$BaTiO_3$ evaluated using SEM in our preceding paper was approximately 1000 nm [26]. The N_2 adsorption isotherms at 77 K in FIG. 1b, were used to evaluate the specific surface areas and micropore volumes, which were determined to be 2 $m^2\ g^{-1}$, 71 $m^2\ g^{-1}$, and 266 $m^2\ g^{-1}$ and 0.000 mL g^{-1}, 0.019 mL g^{-1}, and 0.060 mL g^{-1} for the macro-, meso-, and nano-$BaTiO_3$ crystals, respectively. The particle sizes, which were evaluated under the spherical assumption using the specific surface areas, were determined to be 650 nm, 14 nm, and 4 nm for the macro-, meso-, and nano-$BaTiO_3$ crystals, respectively. The particle size of the nano-$BaTiO_3$ crystals was the smallest because of restriction by carbon nanopores of activated carbon fibers. FIG. 1c, demonstrates that the particle size approximately corresponded to the crystallite size, indicating that the particles were roughly composed of single nanocrystals. The TEM images are shown in FIG. 1d. Nanoparticles of nano-$BaTiO_3$ were observed on a TEM grid and the particle size was 2 nm to 10 nm. The particle sizes of meso- and macro-$BaTiO_3$ was 10 nm to 20 nm and more than 0.5 μm, respectively. Those direct observations of particle sizes approximately agreed with the particle and crystallite size evaluations from the N_2 adsorption isotherms and XRD analyses. In addition, interparticle spaces could form nanopores for those nanoparticles. The nanopore size distribution determined based on non-local density functional theory calculations [30,31] suggested that the nanopores of the nano-$BaTiO_3$ crystals were smaller than those of the meso-$BaTiO_3$ crystals, as observed in FIG. 1e; however, narrow micropores were formed in both the meso- and nano-$BaTiO_3$ crystals. The average nanopore sizes were unexpectedly larger than the particle sizes. Therefore, aggregation of the $BaTiO_3$ crystals occurred and those assemblages then formed relatively large nanopores.

FIG. 2, presents the CO_2 adsorption isotherms at 273 K, 303 K, 333 K, and 363 K. The macro-$BaTiO_3$ crystal exhibited typical ceramic crystallinity and CO_2 was rarely adsorbed on the macro-$BaTiO_3$ crystal surfaces. However, the meso- and

nano-$BaTiO_3$ crystals adsorbed substantial amounts of CO_2 because of the nanocrystallization. Surprisingly, adsorption hysteresis was observed even at 303 K and 333 K, and CO_2 was perfectly released in vacuo at these temperatures. Reversible CO_2 physical adsorption and desorption on porous media were typically observed; however, adsorption hysteresis was observed for adsorbents with chemisorbing species such as amine groups. Therefore, the nano-$BaTiO_3$ crystals exhibited weak chemisorption of CO_2.

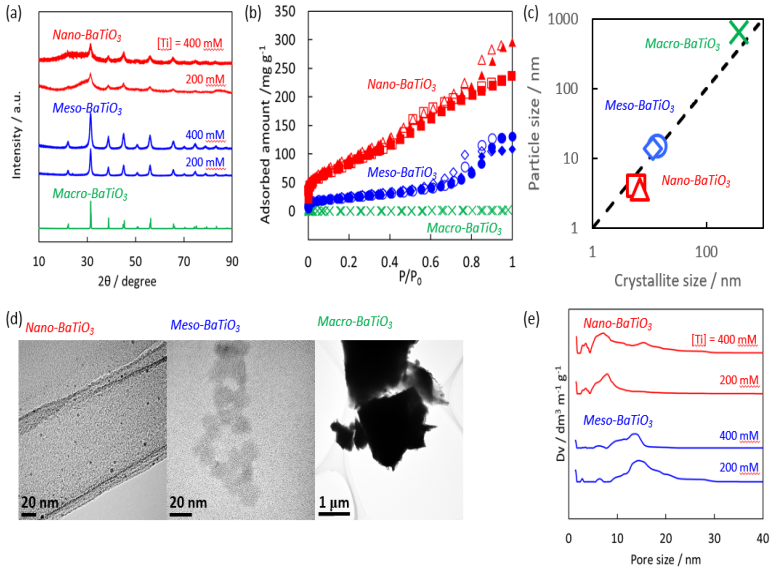

FIG. 1. **Structural evaluation of nano-$BaTiO_3$ (red), meso-$BaTiO_3$ (blue), and macro-$BaTiO_3$ (green) crystals. (a) XRD patterns of nano-, meso-, and macro-$BaTiO_3$ crystals. (b) N_2 adsorption isotherms of $BaTiO_3$ crystals at 77 K for adsorption (filled symbols) and desorption courses (open symbols). Meso-$BaTiO_3$ crystals synthesized using 200 (○) and 400 (◊) mM concentrations and nano-$BaTiO_3$ crystals synthesized using 200 (□) and 400 (△) mM concentrations. (c) Comparison of particle size and crystallite size. (d) TEM images of $BaTiO_3$ crystals. (e) Nanopore size distributions of $BaTiO_3$ crystals.**

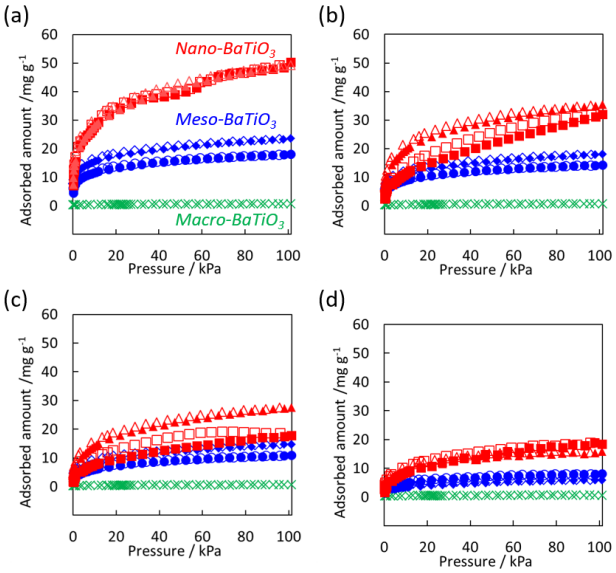

FIG. 2. **CO_2 adsorption isotherms of nano- (red), meso- (blue), and macro-$BaTiO_3$ (green) crystals at 273 (a), 303 (b), 333 (c), and 363 K (d) for adsorption (filled symbol) and desorption courses (open symbol). Meso-$BaTiO_3$ crystals**

synthesized using 200 (○) and 400 (◊) mM concentrations and nano-$BaTiO_3$ crystals synthesized using 200 (□) and 400 (△) mM concentrations.

Considerable adsorption hysteresis of CO_2 adsorption in the nano-$BaTiO_3$ crystals was observed, as mentioned above, especially for the 200 mM concentration. FIG. 3a, shows the adsorption hysteresis areas evaluated based on the difference between the integrals of the adsorption and desorption amounts. The adsorption hysteresis for the nano-$BaTiO_3$ crystals is clearly larger than that for the meso-$BaTiO_3$ crystals. The adsorption hysteresis loop shrunk with increasing temperature except for the nano-$BaTiO_3$ crystals synthesized using the 200 mM concentration. The adsorption hysteresis area for the nano-$BaTiO_3$ crystals had a maximum at 303 K to 333 K. The ratio of the adsorption hysteresis is defined as the adsorption hysteresis area divided by the integral of the adsorption amount, as shown in FIG. 3b. The ratio of the adsorption hysteresis reached a maximum at 333 K, suggesting that the activation energy of CO_2 capture and/or weak CO_2 chemisorption was 333 K. These quasi-irreversible adsorption properties have rarely been observed for CO_2 adsorption on typical porous media.

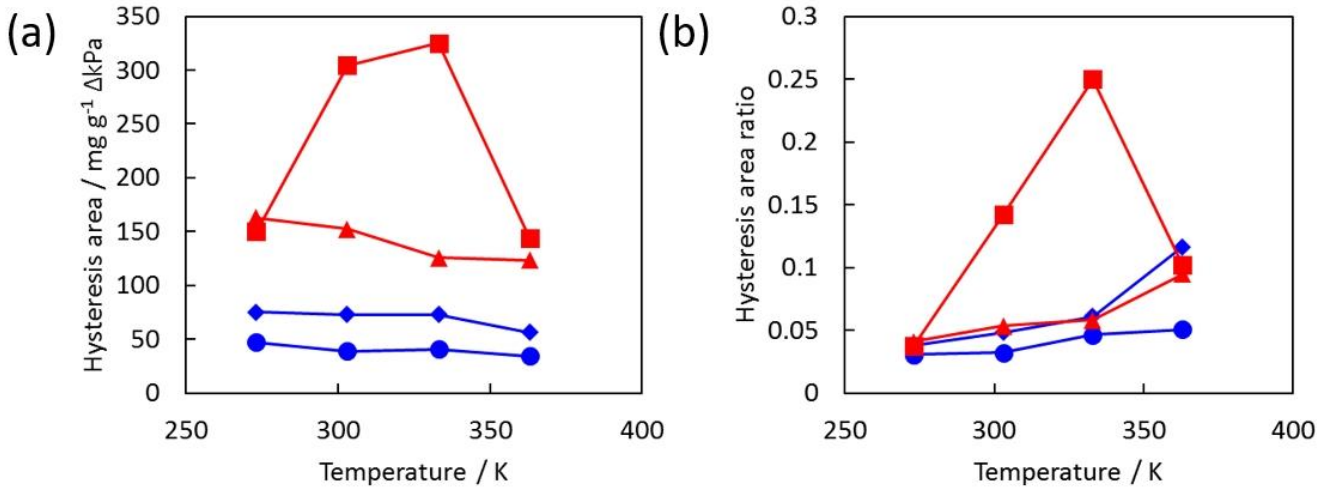

FIG. 3. **Adsorption hysteresis in CO_2 adsorption isotherms at 273 K to 363 K (a) and ratios of adsorption hysteresis areas (b). Meso-$BaTiO_3$ crystals synthesized using 200 (○) and 400 (◊) mM concentrations and nano-$BaTiO_3$ crystals synthesized using 200 (□) and 400 (△) mM concentrations.**

FIG. 4, shows the adsorption density changes at various temperatures. Here, the adsorption densities were calculated based on the adsorption amounts and micropore volumes. The results for microporous media are also shown for comparison because CO_2 could be mainly adsorbed in the micropores. The meso- and nano-$BaTiO_3$ crystals had extremely high adsorbed densities compared with the other microporous media. The adsorbed densities were somewhat maintained even at temperatures above 333 K. The mesopores of the meso-$BaTiO_3$ crystals partially adsorbed CO_2, thereby increasing the adsorbed density. The adsorbed densities in the meso- and nano-$BaTiO_3$ crystals were sufficiently high; the CO_2 solid density at 195 K and liquid density at 236 K were 1560 mg/cm^{-3} and 1100 mg/cm^{-3}, respectively. The specific surface areas and micropore volumes of the meso- and nano-$BaTiO_3$ crystals were relatively smaller than those of typical microporous media. To improve the adsorption performance of CO_2, aggregation of nanocrystals must be prevented.

FIG. 5, presents the XRD patterns of the CO_2-adsorbed meso- and nano-$BaTiO_3$ crystals at 100 kPa, and the meso- and nano-$BaTiO_3$ crystals in vacuo. The XRD pattern of the CO_2 solid is also shown for comparison [32-35]. The differences between the $BaTiO_3$ crystals with and without CO_2 originate from the correlation between CO_2-CO_2 and CO_2-$BaTiO_3$ crystals. The

differential broad peaks were assigned to the CO_2 solid. Thus, the solid-like structure of CO_2 adsorbed in the nanopores of the nano-$BaTiO_3$ crystals was formed. The solid-like structure formation of CO_2 resulted in high adsorption density in the nanopores.

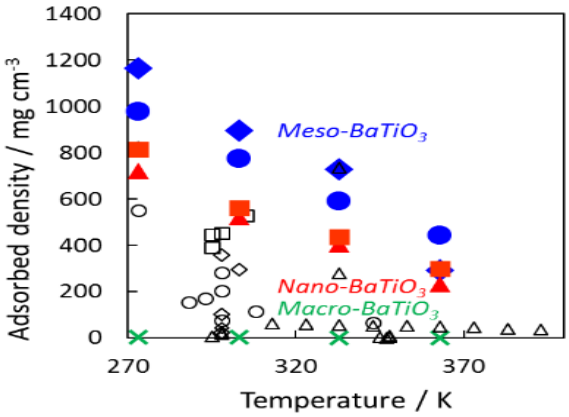

FIG. 4. **CO_2 adsorption densities in nanopores of $BaTiO_3$ crystals and other porous materials at 100 kPa. The nano-$BaTiO_3$ crystals synthesized at concentrations of 200 and 400 mM are depicted by blue circles and diamonds, respectively. The meso-$BaTiO_3$ crystals synthesized at concentrations of 200 and 400 mM are depicted by red triangles and squares, respectively. The macro-$BaTiO_3$ crystal is depicted by green crosses. (○): carbon materials S32], ◊: metal-organic frameworks [9,13,33,34], □: zeolites [10], and ∆: porous silica [32].**

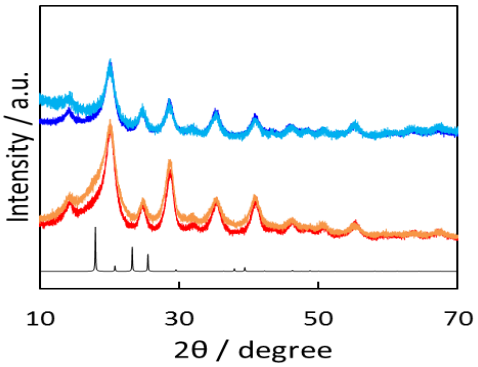

FIG. 5. **XRD patterns of meso-$BaTiO_3$ crystal (dark blue), meso-$BaTiO_3$ crystal adsorbing CO_2 (light blue), nano-$BaTiO_3$ crystal (red), nano-$BaTiO_3$ crystal adsorbing CO_2 (orange), and CO_2 solid (black) at 1 GPa [33].**

Conclusions

In this work, we demonstrated the anomalous CO_2 adsorption properties of nanoscale $BaTiO_3$ crystals. $BaTiO_3$ is a conventional ceramic that exhibits almost non-existent adsorption performance. However, nanocrystallization of $BaTiO_3$ induced high CO_2 adsorption performance associated with adsorption hysteresis and the formation of a solid-like CO_2 structure. $BaTiO_3$ crystals inherently exhibit strong dielectric properties and interact with the partial charges of CO_2, forming a quadrupole moment. The quasi-irreversible adsorption properties on the nano-$BaTiO_3$ crystals are important to adsorb and release CO_2 efficiently, because typical porous solids have weak adsorption potential of CO_2 and chemisorption by amine-functionalized media is too strong to release CO_2. Thus, the fabrication of nanoscale $BaTiO_3$ crystals revealed their excellent

CO_2 adsorption performance. However, some nanoscale $BaTiO_3$ crystals became aggregated, and this aggregation reduced the surface areas. Further study is thus necessary to prevent the aggregation of nanoscale $BaTiO_3$ crystals.

Acknowledgements

We thank Dr. S. Kawaguchi for his help in recording the XRD data at SPring-8. TEM observations were performed at the Chemical Analysis Center, Chiba University. This research was supported by the Japan Society for the Promotion of Science KAKENHI (Grant Numbers 26706001 and 15K12261), research fellowships from the New Energy and Industrial Technology Development Organization (NEDO), Japan, and the Futaba Electronics Memorial Foundation.

REFERENCES

1. Arnette N. Renewable energy and carbon capture and sequestration for a reduced carbon energy plan: An optimization model. Renew Sust Energ Rev. 2017;70:254-65.
2. White CM, Strazisar BR, Granite EJ, et al. Separation and Capture of CO_2 from large stationary sources and sequestration in geological formations: Coalbeds and deep saline aquifers. J Air Waste Manage Assoc. 2013;53(6):645-715.
3. Kangwanwatana W, Saiwan C, Tontiwachwuthikul P. Study of CO_2 adsorption using adsorbent modified with piperazine. Chem Eng Trans. 2013;35:403-8.
4. Songolzadeh M, Ravanchi MT, Soleimani M. Carbon dioxide capture and storage: A General review on adsorbents. WASET. 2012;6(10):225-32.
5. Songolzadeh M, Soleimani M, Ravanchi MT, et al. Carbon dioxide separation from flue gases: A technological review emphasizing reduction in greenhouse gas emissions. Sci World J. 2014;2014:1-34.
6. Choi S, Drese JH, Jones CW. Adsorbent materials for carbon dioxide capture from large anthropogenic point sources. Chem Sus Chem. 2009;2(9):796-854.
7. Li Y, Sun N, Li L, et al. Grafting of amines on ethanol-extracted SBA-15 for CO2 adsorption. Materials. 2013;6:3981-99.
8. Yu CH, Huang CH, Tan CS. A review of CO_2 capture by absorption and adsorption. Aerosol Air Qual Res. 2012;12(5):745-69.
9. D'Alessandro DM, Smit B, Long JR. Carbon dioxide capture: Prospects for new materials. Angew Chem Int Ed. 2010;49(35):6058-82.
10. Lee JS, Kim JH, Kim JT, et al. Adsorption equilibria of CO_2 on zeolite 13X and zeolite X/activated carbon composite. J Chem Eng Data. 2002;47(5):1237-42.
11. Wickramaratne NP, Jaroniec M. Activated carbon spheres for CO_2 adsorption. ACS Appl Mate Interfaces. 2013;5(5):1849-55.
12. Bai BC, Kim EA, Lee CW, et al. Effects of surface chemical properties of activated carbon fibers modified by liquid oxidation for CO_2 adsorption. J S Im Appl Surf Sci. 2015;353:158-64.
13. Mason JA, Sumida K, Herm ZR, et al. Evaluating metal-organic frameworks for post-combustion carbon dioxide capture via temperature swing adsorption. J R Long Energy Environ. 2011;4(8):3030-40.
14. Fauth DJ, Gray ML, Pennline HW, et al. Investigation of porous silica supported mixed-amine sorbents for post-combustion CO_2 capture. Energy Fuels. 2012;26(4):2483-96.
15. Zhao MH, Bonnell DA, Vohs JM. Influence of ferroelectric polarization on the energetics of the reaction of 2-

fluoroethanol on $BaTiO_3$. Surface Sci. 2009;603(2):284-90.

16. Zhao MH, Bonnell DA, Vohs JM. Effect of ferroelectric polarization on the adsorption and reaction of ethanol on $BaTiO_3$. Surface Sci. 2008;602(17):2849-55.
17. Higai S. Remarkable enhancement of adsorption stability for H_2OH_2O and CO_2CO_2 molecules on ceramic $BaTiO_3BaTiO_3$ nanocluster surfaces: Theoretical study. AIP Conference Proceedings. ICCMSE. 2014;1618(2017):1020.
18. Baniecki JD, Ishii M, Kurihara K, et al. Chemisorption of water and carbon dioxide on nanostructured $BaTiO_3$–$SrTiO_3$ (001) surfaces. J Appl Phys. 2009;106(5):054109.
19. Jones PM, and Dunn S. Photo-reduction of silver salts on highly heterogeneous lead zirconate titanate. Nanotechnology. 2007;18(18):185702.
20. Newalkar BL, Komarneni S, Katsuki H. Microwave-hydrothermal synthesis and characterization of barium titanate powders. Materials Research Bulletin. 2001;36(13):2347-55.
21. Pinceloup P, Courtois C, Vciens J, et al. Evidence of a dissolution–precipitation mechanism in hydrothermal synthesis of barium titanate powders. J Eur Ceram Soc. 1999;19:973.
22. Eckert JO, Hung-Houston CC, Gersten BL, et al. Kinetics and mechanisms of hydrothermal synthesis of barium titanate. J Am Ceram Soc. 1996;79(11):2929-39.
23. Frey MH, Payne DA. Grain-size effect on structure and phase transformations for barium titanate. Phys Rev B. 1996;54(5):3158.
24. Hernandez BA, Chang KS, Fisher ER, et al. Sol: Gel template synthesis and characterization of $BaTiO_3$ and $PbTiO_3$ nanotubes. Chem Mater. 2002;14(2):480-2.
25. Meier W, Meyer KE, Sava Gallis DF, et al. Highly textured $BaTiO_3$ via templated grain growth and resulting polarization reversal dynamics. J Am Ceram Soc. 2016;99(3):922-9.
26. Ohba T, Ohyama Y, Kanoh H. A new route to nanoscale ceramics in asymmetric reaction fields of carbon nanospaces. RSC Advances. 2014;4(62):32647-50.
27. Scherrer P. Determination of the internal structure and size of colloid particles by means of X-rays. In Kolloid Chemistry A textbook in 1912 (pp. 387-409). Springer in Berlin Heidelberg.
28. Barrett EP, Joyner LG, Halenda PP. The determination of pore volume and area distributions in porous substances. I. Computations from nitrogen isotherms. J Am chem soc. 1951;73(1):373-80.
29. Dubbinin MM. The Potential Theory of Adsorption of Gases and Vapors for Adsorbents with Energetically Nonuniform Surfaces. Chem Rev. 1960;60(2):235-41.
30. Ravikovitch PI, Vishnyakov A, Russo R, et al. Unified approach to pore size characterization of microporous carbonaceous materials from N~ 2, Ar, and CO~ 2 Adsorption Isotherms. Langmuir. 2000;16(5):2311-20.
31. Neimark AV, Ravikovitch PI, Grün M, et al. Pore size analysis of MCM-41 type adsorbents by means of nitrogen and argon adsorption. J Colloid Interface Sci. 1998;207(1):159-69.
32. Samanta A, Zhao A, Shimizu GK, et al. Post-combustion CO_2 capture using solid sorbents: a review. Ind Eng Chem Res. 2011;51(4):1438-63.
33. Zhang Z, Zhao Y, Gong Q, et al. MOFs for CO_2 capture and separation from flue gas mixtures: the effect of multifunctional sites on their adsorption capacity and selectivity. Chem Commun. 2013;49(7):653-61.
34. Zhang Z, Yao ZZ, Xiang S, et al. Perspective of microporous metal-organic frameworks for CO_2 capture and separation. Energy Environ Sci. 2014;7(9):2868-99.

35. Downs RT, Somayazulu MS. Carbon Dioxide at 1.0 GPa. Acta Crystallogr Sect C Cryst Struct Commun. 1998;54(7):897-8.